Engineering Structures 259 (2022) 114127

Contents lists available at ScienceDirect

Engineering Structures

journal homepage: www.elsevier.com/locate/engstruct

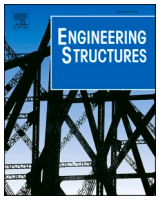

Seismic response of regular multi-span bridges having buckling-restrained braces in their longitudinal direction

Homero Carrion-Cabrera *, Michel Bruneau

Dept. of Civil Structural and Environmental Engineering, University at Buffalo, Buffalo, NY 14260, United States

ARTICLE INFO

Keywords:
Buckling restrained braces
Multi-span bridges
Multimode spectral method
Seismic force reduction factor
Modal response spectrum analysis
Inelastic analysis

ABSTRACT

Buckling Restrained Braces (BRBs) have been used widely in building seismic resisting systems, and have much potential for applications in bridges. One such application is in ductile end diaphragms, a design concept that aims to protect bridge substructures and limit displacement demands by the use of fuse elements, and that can achieve these goals using BRBs. Here, regular, straight, simply-supported, multi-span bridges with BRBs in bidirectional ductile end diaphragms are studied in the longitudinal direction to better understand the behavior of such bridges and correspondingly provide design recommendations (to complement the existing AASHTO design provisions that already address response in the transverse direction for that structural system). Two different layouts of implementation were studied, and designed using the multimode spectral method to identify their respective benefits. A parametric study was conducted on the preferred configuration in which BRBs were used to connect spans to piers, using nonlinear response history analysis to understand the influence of pier stiffness, BRB yield displacement, target BRB ductility demand, and other factors on overall inelastic response. Overall, the use of BRBs was found to effectively limit the displacement demands in columns and expansion joint opening, achieving the structural fuse objective. These dynamic analyses allowed to understand the impact of many parameters on longitudinal response and behavior of the type of bridges considered, which led to a proposed design procedure for BRBs used in this configuration.

1. Introduction

Buckling restrained braces (BRB) are special braces capable to yield in axial tension and compression. They allow to achieve large plastic displacements, produce stable hysteretic behavior, and dissipate large amounts of seismic energy – capabilities that are valuable in seismic resisting structures. Initially, these elements were first introduced in buildings in Japan in 1987, in the USA in 1999 [1], and in many other countries since. They are nowadays widely used and design requirements for buckling restrained braced frames are specified by the AISC Seismic Provisions for Structural Steel Buildings [2]. Given that all the yielding in a BRB happens inside its casing, to help structural engineers determine if BRBs should be replaced following an earthquake, some manufacturers have also integrated into their BRBs displacement transducers capable of recording the history of cyclic deformations of the brace yielding core over time; this information can then be used to calculate the BRB remaining fatigue life and avoid premature replacement after major earthquakes and/or several years of services. In bridges, there have been much fewer applications to date. Examples include the Vincent Thomas Bridge [3] and the Minato bridge [4] which were retrofitted with BRBs. While these were large bridges that were analyzed using Nonlinear Response History Analysis (NL-RHA), there would be benefits in using BRBs to enhance the seismic performance of common bridges, particularly if they could be designed using elastic procedures.

In bridges, before the use of BRBs, several concepts were developed to implement hysteretic energy dissipation devices. One such concept that is considered here is the use of ductile end diaphragms, which consists of hysteretic devices (or "structural fuses") implemented in the diaphragms located at the ends of spans. These ductile end diaphragms are intended to dissipate seismic energy and prevent damage in the substructure by limiting the magnitude of transmitted forces. The concept was initially developed and tested with various hysteretic devices for seismic forces in the transverse direction by Zahrai and Bruneau [5] and a design procedure provided by Alfawakhiri and Bruneau [6] has been implemented in AASHTO [7]. Further shake table studies verified the concept by exciting, in their transverse direction, scaled bridges having BRBs as fuse elements at their end diaphragms [8]. Later,

* Corresponding author.
E-mail addresses: homerofe@buffalo.edu (H. Carrion-Cabrera), bruneau@buffalo.edu (M. Bruneau).

https://doi.org/10.1016/j.engstruct.2022.114127
Received 12 March 2021; Received in revised form 10 February 2022; Accepted 8 March 2022

the concept was expanded to bidirectional seismic forces for bridges with stiff structures [9,10] and a design procedure was also provided for the case of rigid piers. The concept of bidirectional ductile end diaphragm emphasizes the ability to dissipate energy under both longitudinal and transverse seismic excitations. The advantage of this system is the restriction of displacements between spans, which can be accommodated with low cost expansion joints, and the prevention of damage to substructural elements when bridges are seismically excited in both horizontal directions. Pantelides et al. [11] studied the application of BRBs in the longitudinal direction to reduce pounding in curved and skewed bridges as a retrofit strategy but did not propose a generally applicable elastic analysis based design procedure.

Currently, if wishing to use BRBs to implement a bidirectional diaphragm strategy, AASHTO provides simple equations that could be used for the transverse direction, but there is no verified procedure available other than performing NL-RHA to design BRBs in the longitudinal direction. Here, bridges having BRBs acting in the longitudinal direction and installed at the ends of their spans are studied to understand their overall behavior and the properties required to improve their seismic performance, and findings from these analyses are used to provide guidance on their design using elastic procedures. Additionally, research was conducted to investigate whether the multimode spectral method (described in AASHTO [7,12]) is an appropriate analysis method that could be used to predict the longitudinal ductility demand and response of bridges having BRBs as part of this ductile diaphragm strategy.

As a first step to investigate the application of bidirectional ductile end diaphragms, the focus here is on regular straight simply-supported multi-span bridges having from 2 to 11 spans, implemented with BRBs in the longitudinal direction, and with spans supported by bidirectional sliding bearings. The bearings are assumed to have negligible lateral strength and to be supported on rigid abutments and elastic piers. This is consistent with the targeted seismic performance of keeping the substructure and superstructure elastic while BRBs behave inelastically, limiting maximum forces in the structure. Further research will consider different and more complex bridge archetypes and geometries, which are beyond the scope of this paper.

2. Buckling restrained braces

Although a detailed history of the development and past research on BRBs is beyond the scope of this paper, a brief overview of some of this past work is provided here to highlight relevant research done on this topic and emphasize that applications in bridges are relatively new.

BRBs were first developed in Japan in the 1970s [13] and have been implemented in buildings in the U.S. since 1999 [14]. Several studies have focused on the behavior, design, and application of BRBs in buildings. In particular, research has focused on providing guidelines on how to design the BRB casing [15] as well as the BRB end-connection details to ensure the stability of the brace [16,17]. This includes studies to investigate the properties of various connections and methods to verify the stability of the brace [18–20]. Different methods to build effective BRBs were also proposed, with some BRBs using a steel case filled with concrete, some without concrete, and even some with alternative materials (such as using a wood case, among others [21–23]). Note that some types of BRB are proprietary, and others are not. More recent studies have also investigated whether their replacement is necessary after an earthquake, by considering their low cycle fatigue and developing equations to quantify the damage in the brace due to an earthquake [24], thereby increasing the reliability of these elements. In short, BRBs have been studied for more than 4 decades, and because they are nowadays commonly used in buildings, most of the research has focused on this application [25–31]. The few applications to date in bridges have been described in the introduction.

For the type of BRBs most commonly used worldwide and contemplated for the current applications in bridges, BRBs usually consist of a steel plate (wrapped in an unbonding material) inside a casing filled with concrete [15] that provides support to the steel plate to prevent its buckling under compressive forces, allowing it to reach yielding in compression [13,15]. The steel core has three main segments: the restrained yielding segment, the restrained nonyielding segment, and the unrestrained nonyielding segment. The BRB axial stiffness, K_{BRB}, is calculated using Eq. (1) where E_s is the steel elastic modulus, L and A are the length and cross-section areas, and subscripts y, ur, and uu represent the restrained yielding segment, the restrained unyielding segment, and the unrestrained unyielding segment, respectively. However, at design time, BRB geometry is unknown; thus, as a simplification, the stiffness can be obtained using Eq (2) where L_{eq} is an equivalent length that is larger than the length of the yielding core.

$$K_{BRB} = \frac{E_s}{\frac{L_y}{A_y} + 2\frac{L_{ur}}{A_{ur}} + 2\frac{L_{uu}}{A_{uu}}} \tag{1}$$

$$K_{BRB} = \frac{A_y E_s}{L_y} \frac{1}{1 + 2\frac{L_{ur}}{L_y}\frac{A_y}{A_{ur}} + 2\frac{L_{uu}}{L_y}\frac{A_y}{A_{uu}}} = \frac{A_y E_s}{L_{eq}} \tag{2}$$

The yielding force, P_y, is controlled by the cross-section area of the yielding segment (which from here on is called the BRB area) and the steel minimum yield stress, F_y, such that

$$P_y = A_y F_y \tag{3}$$

and the yield displacement, Δ_y, is

$$\Delta_y = \frac{P_y}{K_{BRB}} = \frac{F_y E_s}{L_{eq}} \tag{4}$$

Due to the relation between Eq. (2), (3), and (4), only two parameters of the three (Δ_y, P_y, K_{BRB}) are required to define the range of elastic behavior. For convenience, the yield displacement is taken here as the known parameter and the yielding force is the one to be determined. Additionally, when using a given material for the BRB (arbitrarily assumed to be a Gr 50 steel here), the problem reduces to finding the cross-section area of the BRB. Note that the BRBs cross-section area can be fabricated to match any needed area value, usually larger than 323 mm^2 (0.5 in^2), and the desired value of yield displacement can be obtained by varying the length of the yielding core.

Failure of a well-designed BRB can occur when reaching its maximum elongation range in compression or due to fatigue after several cycles of inelastic behavior. To minimize these risks of failures, the AISC 341 [2] requires cyclic qualification testing to a maximum displacement equal to twice the design displacement, and the development of a total cumulative plastic displacement equal to 200 times the yield displacement. The maximum elongation can be related to the maximum ductility in the BRB, which depends on the internal design. An adequately designed BRB can sustain large core strains over multiple cycles; for example, Lanning et al. [32] tested BRBs where the core reached a ductility of 30 and cumulative plastic deformation that far outperformed the AISC 341 requirement. Note that using cumulative ductility to establish satisfactory cyclic performance is not the same as using a rigorous low cycle fatigue calculation, which depends on maximum peak displacements and history of displacements, but it is nonetheless a useful indicator of the ductile capacity of the device. Assuming that 30 is the maximum ductility demand that can be developed in a BRB, and assuming that this value would correspond to the AISC-specified value of twice the design displacement in its test protocol, this would imply that it would be reasonable to limit the design ductility demand to values less than 15.

3. BRBs configurations in bridges and expected behavior

BRBs can be implemented in bridges in the longitudinal direction in several different configurations, each resulting in different ductility demands. Two configurations were studied here: Configuration 1, with

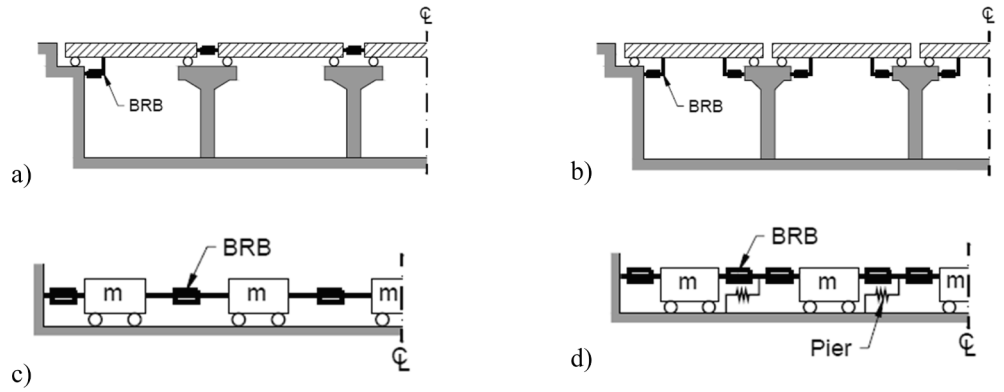

Fig. 1. Bridges considered: a) Configuration 1; b) Configuration 2; c) Model for Configuration 1; d) Model for Configuration 2.

BRBs connecting to spans between each other, as shown in Fig. 1a; and Configuration 2 where BRBs connect spans to the substructures, as shown in Fig. 1b. An "ideal" seismic performance is defined here as the condition when a relatively uniform ductility demand is reached in all BRBs along the bridge, and with values close to a specific target ductility demand. These ductilities in BRBs develop as a consequence of the relative displacement demands between spans, and between spans and their supports (where supports would only be abutments for Configuration 1). Note that since BRBs are connected between superstructure and substructures, spans are no longer free to expand or shrink due to temperature. This implies that, during the bridge's lifetime, BRBs will experience several cycles of temperature-induced strains that must be considered when calculating their fatigue life. Nevertheless, the temperature issue has been shown to be manageable following procedures described elsewhere [33], and is beyond the scope of the current paper.

The nonlinear performance expected in each configuration is to limit yielding to the BRBs such as to prevent all damage in the substructure and superstructure, similarly to the performance expected in essential or critical bridges. As stated earlier, it was also deemed desirable that BRBs reach the same target ductility along the bridge. After consulting with BRB suppliers to assess what would be a large but workable value for this target design value, it was decided to set the design ductility demand here to 10. Note that, for the structures proposed, an infinite number of different design solutions can be obtained by tuning the properties of BRBs, for instance varying the yield displacement or the yield strength of some or all of the BRBs along the bridge. For simplicity here, all the BRBs along the bridge were considered to have the same yield displacement.

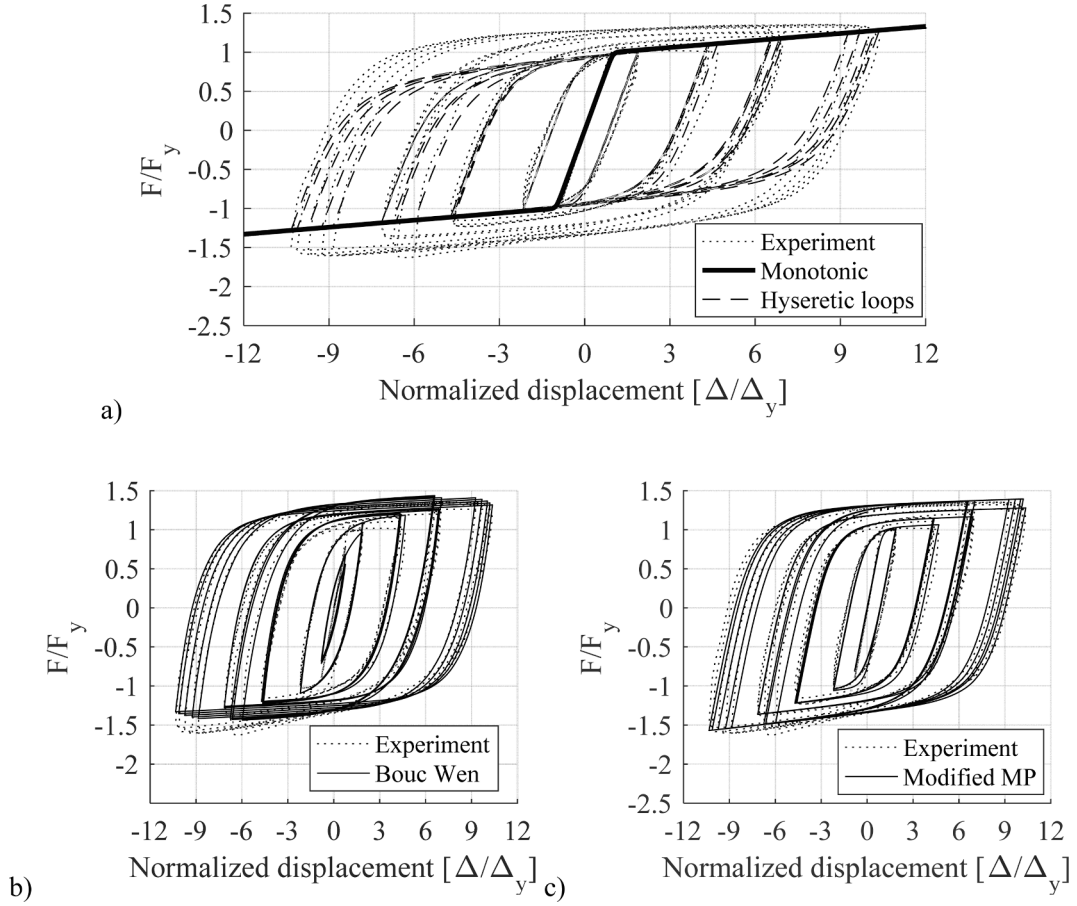

Fig. 2. Hysteretic behavior of BRB with different models: a) Menegotto Pinto; b) Bouc Wen; c) Menegotto Pinto with isotropic hardening.

4. Numerical model

In the current study, since analysis was only performed in the longitudinal direction and P-Δ effects in piers were not considered, the bridges could be treated as unidimensional models. These models represent regular simply-supported multi-span bridges with spans supported at their ends by sliding bearings having negligible lateral strength and located at the top of abutments or piers. Spans are considered axially rigid in the longitudinal direction and since the model is unidirectional, knowledge of their length is not required. Each span mass is therefore represented by a lumped mass connected to the BRBs. Abutments were considered rigid and located at the ends of the bridge. Note that in practice several BRBs in parallel could be connected at the end of one span; all those BRBs are represented here as one equivalent BRB, with identical BRBs yield displacement and strength equal to the total strength of the group. BRBs were modeled as truss elements. As a result, bridges were modeled as masses and springs as shown in Fig. 1c and 1d. Using as a reference bridge drawings provided to the authors by the California Department of Transportation, the pier mass was approximated as 10% of the span mass and lumped at the top of the pier. For a given bent, this mass represents the mass of the cap beam and half the mass of the columns lumped at the top of the pier. Piers were modeled as springs with stiffness representative of vertical cantilever elastic elements fixed at their base.

For NL-RHA, three different non-linear models were used to compare behavior. First, the Menegotto Pinto model was used without isotropic hardening and with 3% post elastic stiffness to represent a general BRB backbone curve [3]; the monotonic and hysteretic behavior of this steel model is shown in Fig. 2a. Then, the Bouc Wen model [34,35], and the Menegotto Pinto model modified by Filippou [36] were used (the latter is an upgrade of the Menegotto Pinto that allows to model unsymmetrical hysteretic curves and is implemented in OpenSees [37] with the material name SteelMPF); hysteretic curves for both models are shown in Fig. 2b and 2c comparing with experimental results for BRBs. All models were selected because they have a smooth transition from elastic behavior to plastic behavior, which was deemed to be representative for BRBs (and also has been reported advantageous to avoid large spurious damping forces [38]). Parameters for each of these models used in OpenSees are listed in the appendix.

In the following NL-RHA, the Menegotto Pinto model was used, with results selectively compared later using the other two models. In all cases, Rayleigh Damping was used with 5% of critical damping set at the first and third mode. The 5% value was used to indirectly account for some minor bearing friction, nonlinear behavior of piers, and radiation damping at the foundation of piers. Finally, nonlinear analysis was performed in OpenSees and result post-processing was performed in MATLAB [39].

5. Seismic hazard and ground motions

The design spectrum used in this study corresponds to Memphis, Tennessee. This location was selected for consistency with previous work by Wei and Bruneau 2016. For the NL-RHA performed in this study, a few sets of ground motions were considered along with different scaling procedures. The FEMA P695 [40] far-field set of ground motions was eventually selected and used, along with its ground motion scaling procedure. It consists of 22 pairs of ground motions selected to represent a variety of locations and seismic hazards. This set was used because it is not site dependent, and the FEMA P695 scaling procedure was used here as it is accepted and not overly-conservative. Incidentally, among all the possible scaling procedures considered as part of this project, it was found to generally produce a lower median and variation in the resulting ductility demands.

6. Definition of parameters

A limited-scope parametric study was first conducted to provide some insights on the behavior of multi-span bridges with BRBs in the longitudinal direction. The parameters to be analyzed were obtained from the equation of motion normalized following a procedure similar to the one used by Mahin and Lin [41]. The resulting normalized equation of motion considering a Caughey [42] damping model is

$$[M_n]\left\{\ddot{u}_n\right\} + \overbrace{[M_n]\sum_b a_b\left(\frac{K_p}{m_s}[M_n]^{-1}[K_{Tn}]\right)^b}^{[C_n]}\left\{\dot{u}_n\right\} + \frac{K_p}{m_s}\left\{f_{sn}(\{u_n\})\right\} = -\left(\frac{\ddot{u}_{g_{max}}}{\Delta_{y_{BRB}}}\right)[M_n]\{\iota\}\frac{\ddot{u}_{g_n}}{\ddot{u}_{g_{max}}} \tag{5}$$

where $[M_n]$, and $[C_n]$ are respectively the mass and damping matrix normalized by span mass, m_s; $[K_{Tn}]$ is the tangent stiffness matrix normalized by pier stiffness, K_p; $\{u_n\}$ is the vector of nodal time history displacements normalized by the BRB yield displacement, Δ_y, and dots above variables represent time derivatives; $f_{sn}\{u_n\}$ is the vector of restoring forces normalized by the product $K_p\Delta_y$; $\{\iota\}$ is the influence vector; $\ddot{u}_g$ is the ground acceleration time history; $\ddot{u}_{g_{max}}$ is the peak ground acceleration, and; b and a_b are Caughey model constants. Note that the Caughey damping model is a general model to represent classical damping matrices, and Rayleigh damping is a simplified case of this model. The equation shows that for a given ground motion and BRB yield displacement, the response displacement history of all nodes will be the same for all bridges that have the same normalized matrices $[M_n]$ and $[K_{Tn}]$, and have the same ratio between pier stiffness and mass span. In the case when the ground motion is scaled, the response in terms of normalized displacement does not change if the BRB yield displacement is scaled in the same proportion. The ratio K_p/m_s can be also represented by the period of the pier, T_p, that has a physical meaning and is defined as:

$$T_p = 2\pi\sqrt{\frac{m_s}{K_p}} \tag{6}$$

where T_p increases when the pier stiffness reduces and reduces when the pier stiffness increases.

As a result of the above equation of motion formulation, parameters to be considered in the parametric study were defined. Different numbers of spans and different BRB target ductility demands were considered. The ductilities were obtained as a result of various R values used in designing the BRBs, where R is the seismic force response modification factor (defined in many design codes and standards, including AASHTO for example). The span mass for all bridges and the design spectrum were assigned to remain constant in this study because the effect of their variation can be equivalently accounted by varying other parameters instead, such as the pier stiffness and the BRB yield displacement, respectively. To investigate the response of a range of regular bridges, different values of pier stiffnesses and BRB yield displacements were considered. For this parametric study, the number of spans ranged from 2 to 11, the span mass was arbitrarily set equal to 175.55 Mg (1 $kip{\cdot}s^2/in$), the piers stiffness ranged from 1.76 kN/mm (10 kip/in) (representing a flexible pier) to 702.22 kN/mm (4000 kip/in) (representing a rigid pier), the ratio of the mass of the pier to the span mass was set equal to 0.1, and the yield displacement of the BRB was initially set equal to 3.505 mm (0.138 in). Such yield displacement was represented by a BRB with an equivalent length equal to 2032 mm (80 in) and a Gr 50 steel (a length calculated to be adequate to prevent low-cycle fatigue under annual thermal cycles [33] for an arbitrary span length equal to 30.48 m (100 ft)). Later in this paper, yield displacement values of 1.753 mm (0.069 in) and 7.01 mm (0.276 in) are also considered for comparison purposes. These yield displacements

Table 1
Summary of parameters.

Parameter	Values
Number of spans	2 to 11
Span mass	175.55 Mg (1 $kip{\cdot}s^2/in$)
Pier mass to span mass ratio	0.1
Pier stiffness range	1.76 to 702.22 kN/mm (10 to 4000 kip/in)
BRB yield displacement	3.505, 1.753, 7.010 mm (0.138, 0.069, 0.276 in)

represent BRBs with equivalent lengths equal to 1016 and 4064 mm (40 and 160 in), and with a Gr 50 steel. Values for all these parameters are summarized in Table 1.

7. Elastic design and behavior

Bridges were designed with the multimode spectral method (MM) following the procedure described in AASHTO [7,12]. This method, which is based on a modal response spectral analysis, was selected because of its reported better correlation between MM and NL-RHA in conventional bridges (without BRBs) [43]. The complete-quadratic-combination (CQC) rule was used because it is applicable when structures have both closely separated periods and well separated periods, as in the bridges considered here. Finally, the displacement amplification factor was not considered here to avoid initial bias in results and the predicted BRB ductility demands were calculated as being the ratio of the elastic deformation to the BRB yield displacement.

The design procedure required several iterations until convergence to the final design (i.e., to find the final BRB areas). Iterations were required because the behavior of the structure changes with variations in BRB stiffness and strength. Therefore, a script was implemented in MATLAB. Initially, the function *fminsearch* (MATLAB native function) was used as the algorithm to find the solution. This algorithm required a large number of iterations especially when the piers were more flexible, and in some cases, depending on the convergence parameters and the initial BRB areas used, an ideal solution was not found. To reduce the number of iterations and improve convergence, the algorithm was changed to the secant method (i.e., a method similar to Newton Raphson but instead using secant properties of the results from one iteration to another) and constraining the maximum absolute variation of the new area of any BRB to be approximately equal to 70% of its area in the previous iteration. The algorithm is similar to what is done in non-automated design by trial and error, where areas are reduced if deformations or forces are small, and increased otherwise, until convergence is reached. Moreover, since the system to solve is nonlinear with multiple variables where each variable represents a BRB area, only one variable was varied at the time and 2 iterations were used before changing to the next variable; the process continued until a solution was found for all variables. As a result, a smaller number of iterations was required to converge to the solution.

For example, for BRBs connected to the span closest to the abutment in an n-span bridge, where BRB 1 connects the span to the abutment and BRB 2 connects the span to the pier (Configuration 2) or to the adjacent span (Configuration 1), and the equivalent length is equal to 2032 mm (80 in), the design algorithm is as follows:

1. Provide initial areas to all BRBs in the bridge; all these areas are called the “set of areas”.
2. Calculate forces and deformations using MM; the resulting forces for all the BRBs are called the “set of forces”, and the resulting deformations for all BRBs are called the “set of deformations”.
3. BRB1 is first selected for the design iterations.
4. Iterations begin.
   - 4.1 The area of BRB and the resultant deformation are saved as A0 and D0, respectively. If the BRB deformation is between 99% and 101% of the BRB yield displacement, which for this case is 3.505 mm (0.138 in), then go to step 5; otherwise, for this BRB a new area is calculated by dividing the force in the element by the yielding strength of the core plate, which in this case is equal to 345 MPa (50 ksi). If this new area is in the range between 30 % and 170 % of the BRB area A0, it is selected as the value for the next iteration; otherwise, the range boundary closest to the calculated area is selected. The set of areas is updated with the selected area as the area for the BRB that is been designed.
   - 4.2 Deformation is calculated again using MM for the BRB; the area of BRB and the resultant deformation are saved as A1 and D1, respectively.
   - 4.3 If the BRB deformation is between 99% and 101% of the BRB yield displacement, then go to step 5; otherwise, a new BRB area is calculated with a linear function passing through the points (A0, D0) and (A1, D1) for a deformation equal to the BRB yield displacement. If this new area is in the range between 30 % and

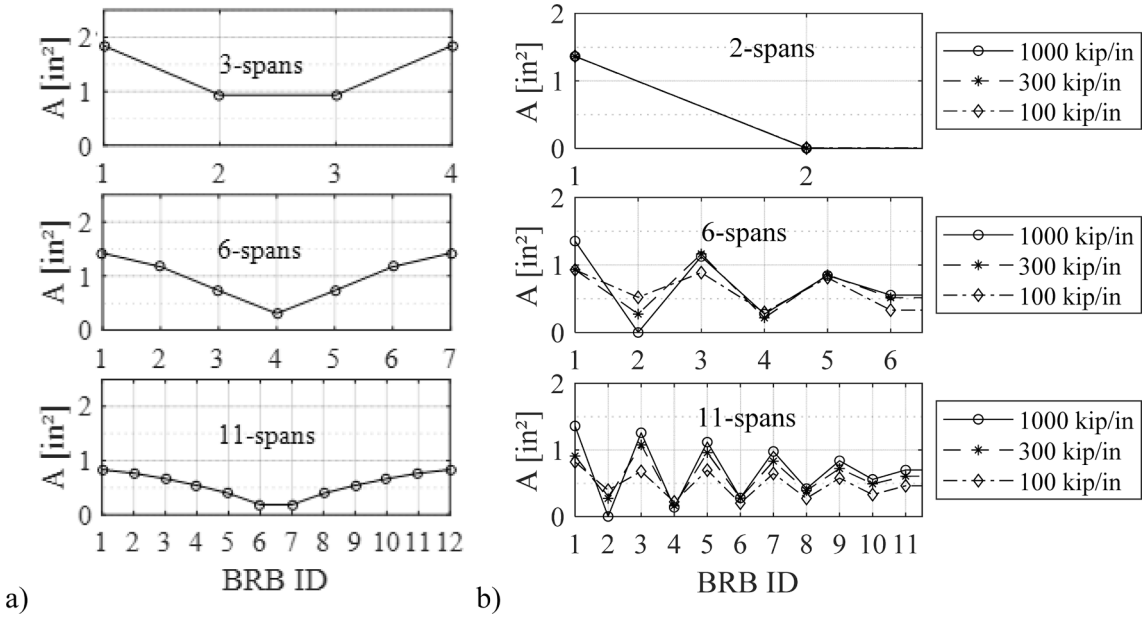

Fig. 3. BRB cross-section areas obtained with RSA for: a) Configuration 1; b) Configuration 2 with different pier stiffnesses.

170 % of the BRB area considered A1, it is selected for the next iteration; otherwise, the range boundary closest to the calculated area is selected. The set of areas is updated with the selected area of the BRB that is been designed.

4.4 Save A1 as A0, and D1 as D0.

4.5 Repeat steps in the following sequence: 4.2, 4.3, and 2. Note that each BRB being designed probably does not immediately converge into the final solution in a given iteration, but rather achieves a better approximation for that step of the iteration process, which is acceptable since other BRBs along the bridge still need to be designed through the other iterations. Usually, convergence to the final solution for the entire set of BRBs is achieved after reaching step 7.

5. Next BRB is selected. For this example, this next BRB would be BRB2. Step 4 is repeated using information for this new considered BRB.
6. Repeat step 5 until all BRBs are selected.
7. Repeat steps 3 to 6 until the variation of the BRB deformation is less than 1% of the BRB yield displacement, or for a maximum of 15 iterations. If the number of iterations is reached, check the results and determine whether it is necessary to go back to step 1 with a different choice of initial area.

For the elastic analysis, the yield displacement was considered equal to 3.505 mm (0.138 in), and the seismic force reduction factor (defined in AASHTO) was set arbitrarily equal to 5, which is the maximum value permitted by AASHTO LFRD [12]. Then the bridge was analyzed as a multi-degree-of-freedom (MDOF) system.

7.1. BRB areas in configuration 1

For this configuration of BRBs, bridges with number of spans ranging from 2 to 11 were designed. BRB areas resulting from the above optimization process are shown in Fig. 3a, for a few bridges. Note that BRB 1 is the one connected to the left abutment and BRBs 4, 7, and 12 are the ones connected to the right abutment for the 3-span, 6-span, and 11-span bridges, respectively. For bridges having an even number of spans (such as the 6-span bridge in Fig. 3a), it was observed that the force in the BRB at the center of the bridge was always zero, irrespectively of the BRB area; hence, for that BRB, because no change in BRB elongation occurred, the initial area provided in the first step of the optimization algorithm never changed (this arbitrary initial value is the value plotted in Fig. 3a). Moreover, for all bridges, it was observed that the resulting BRB area progressively reduced as a function of the distance of the BRB to the center of the bridge, with larger areas for the BRBs located at the abutments, and the smallest areas for those BRBs closer to the center of the bridge. This is logical as all of the bridge seismically-induced inertia forces are transferred to the abutments in this configuration.

7.2. BRB areas in configuration 2

In this case, initially, in addition to considering bridges with a varying number of spans, three different pier stiffness values were used, namely 175.55, 52.67, and 17.56 kN/mm (1000, 300, and 100 kip/in). The resulting BRB areas obtained from the above design approach are shown in Fig. 3b; since the bridges are symmetric, only the resulting BRB areas for the left half of the bridges are presented. As before, BRB 1 is the one connected to the left abutment. Note that results for the 2-span bridge are included here to explain its special case. For the 2-span bridge, all the seismic force was taken by the BRBs connected to the abutments. Hence, in this case, the bridge essentially behaved as two Single-Degree-of-Freedom (SDOF) systems in which pier stiffness does not have any influence. For bridges with 6 and 11 spans, it was observed that the curve showing the variation of BRB areas along the length of the bridge followed an irregular line of alternating peaks and valleys (like a zigzag) as the value of areas increased and decreased. It was peculiar

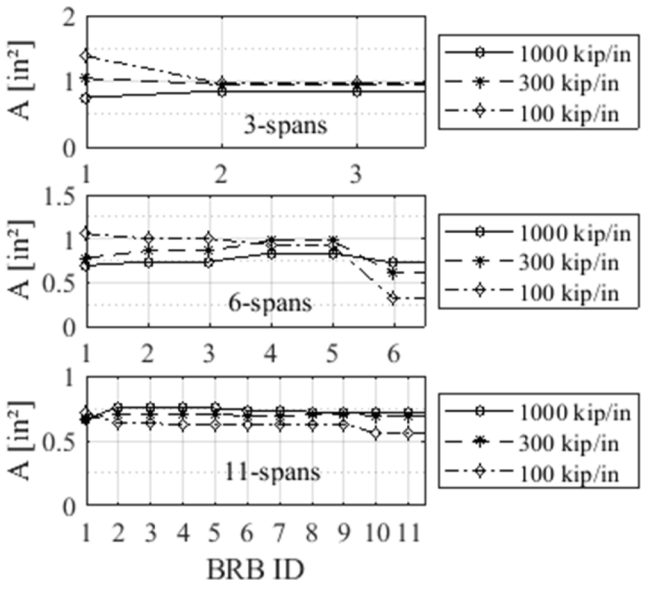

Fig. 4. BRB cross-section areas obtained with RSA for bridges with piers and BRBs connecting to the same pier having the same area.

that the area for the second BRB was zero or approaching zero in models with more stiff piers (although not shown in the figure, this was also the case for the second to last BRB, because of symmetry). Also, it was noticed that the areas obtained across the spans did not exhibit a definite trend in relation to the increase in pier stiffness (for example, in some BRBs, the area increased with stiffer piers, while, in others, the area decreased).

To eliminate the zigzag pattern observed in Fig. 3b, it was found effective to impose an additional constraint to the BRBs cross-section area as part of the optimization process. Of the few options considered, the best solution was to require that BRBs connected to the same pier have the same area. Fig. 4 shows results for BRB areas in bridges designed per this option, where resulting BRB areas connected to the abutment are smaller than those obtained in Configuration 1 and shown in Fig. 3b. As a result, this option transfers less force to the abutment. In general, results indicate that connecting each span with BRBs to their adjacent piers better distribute the seismic demand along the entire length of the bridge if the additional constraint is used. Therefore, this design constraint was retained for all other analyses presented in the rest of the paper.

7.3. Observations from modal response

Some of the above results can be explained in part by observed modal response characteristics. For the regular bridges studied here, the first mode shape has all masses moving in the same direction (e.g., in Fig. 3 all masses move to the right representing a positive value), which implies that all modal displacement values have the same sign, which in turn implies an anti-symmetric deformed shape with respect to the center of the bridge. The second mode has positive values for one half of the bridge, negative values for the other half, and zero displacement at the center node – and therefore, a symmetric deformed shape. The third mode is anti-symmetric, the fourth mode is symmetric, and so on. As a result of the symmetry of the structure and constant span mass, all the symmetric modes (i.e., the even-numbered modes) have a mass participation factor equal to zero.

For bridges with an even number of spans, the center of the bridge is located on the vertical axis of the central pier. The displacement of spans adjacent to that pier will have the same value and same direction for all odd-numbered modes (anti-symmetric deformed mode shapes); as a result, the distance between the two spans meeting at the center of the

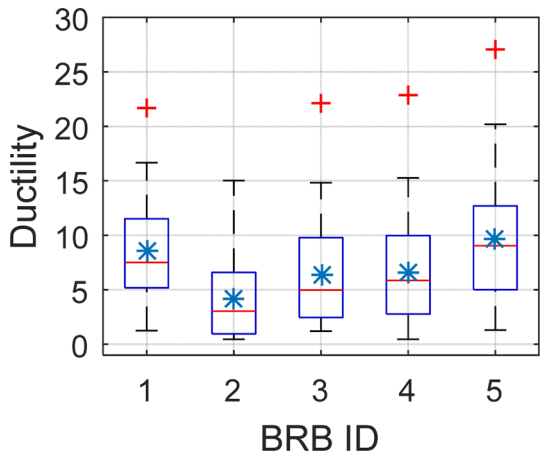

Fig. 5. Scatter in BRB ductility demands from NL-RHA for a 5-span bridge (due to symmetry, results for only half of the bridge are shown).

bridge remains constant. In Configuration 1, the BRB connecting these two spans will therefore experience no elongation, irrespectively of its stiffness. For that reason, the algorithm did not converge to a solution for that BRB, which explains the observations made for even spans and the results in Fig. 3a at the center of the 6-span bridge. In Configuration 2, the behavior of BRBs between spans depends on the stiffness of the pier to which they are connected. If the pier is rigid, both BRBs at the center of the bridge can reach their target ductility (based on the ductility predicted with MM) with the optimization process. However, if the pier is infinitely flexible, the case becomes effectively equivalent to Configuration 1, as both spans will experience pure translation (equal to that of the pier) with no relative displacement between each other and no BRB elongation (unless the BRB stiffness is zero). Consequently, the area for BRBs at the mid-length of bridges with an even number of spans will be small for flexible pier and will reduce to zero for the case of an infinitely flexible pier. This explains the results for the 6-span bridge case in that figure, where cross-section areas of the BRBs located at the center of the bridge are observed to decrease when pier stiffness reduces. In the special case of the 2-span bridge, where the displacement of the spans is limited by the elongation required to reach the target ductility in the BRBs connected to the abutments, the relative displacement between the span and the pier is equal to the elongation in the BRB connected to the abutment; as a result, the BRBs connected to the pier will always have zero stiffness because they are irrelevant, which explains the result shown in Fig. 3b.

For bridges with an odd number of spans, the center of the bridge is located in the middle of the central span. For odd-numbered modes, the modal displacement for spans adjacent to the center span is the same, but different from the modal displacement at the center span. Therefore, in these cases, the BRBs can be tuned to reach their target ductility (based on the predicted ductility with MM). This is valid for both Configurations 1 and 2.

8. Nonlinear analysis

Bridges with the preferred configuration (i.e., Configuration 2) and designed per the above multimode spectral method were evaluated using NL-RHA to determine their behavior and their actual demands. Bridges with 3, 5, 7, 9, and 11 spans were re-designed using the same elastic analysis optimization procedure described above, but using different values of the seismic force reduction factor, R, and BRB yield displacement. In the following sections, after defining demands, the behavior observed for BRBs, columns, and expansion joints is described, the sensitivity of results with respect to the BRB material model is addressed, and the influence of the BRB yield displacement is investigated to better understand the actual ductility demand in BRBs. This was done to help determine how to define the target ductility demand and its relation with the reduction factor to be used in this design.

8.1. Definition of demands

The seismic response of bridges was calculated for the same 22 pairs of ground motions described previously, and scatter in the resulting BRB ductilities was computed. For instance, Fig. 5 shows the ductility demands, μ, for each BRB in a 5-span bridge (the same one shown in Fig. 1b) as boxplots to visualize the range in results. In these boxplots, the line in the middle of the box represents the median of ductilities obtained, the asterisk represents the average value, the top and the bottom of the box represent the 75th and the 25th percentile values, respectively, the horizontal at the top and bottom represent 1.5 times the interquartile distance (i.e., the height of the box) of the box above it or below it, respectively; and finally, the crosses are all obtained extreme values that exceed the 1.5 times the interquartile distance. Recall that, in this 5-span bridge, BRB 1 is connected to the abutment, BRBs 2 and 3 are connected to Pier 1, and BRBs 4 and 5 are connected to Pier 2. For each BRB, the design demand could be defined as the 50th percentile (i.e., the

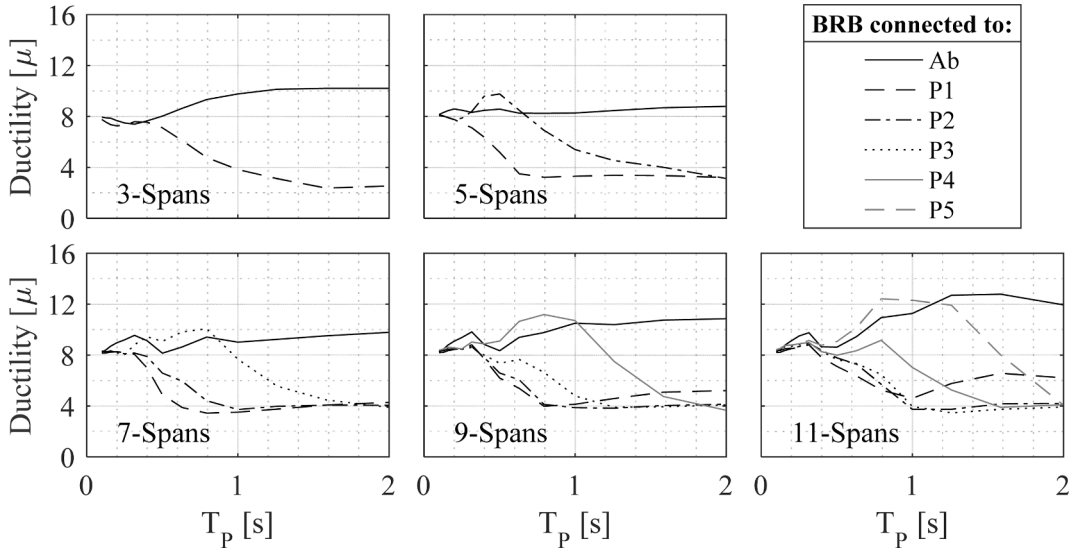

Fig. 6. Ductility demands for Designs with MM and R = 4. (Ab. = abutment, PN = Nth pier next to the abutment).

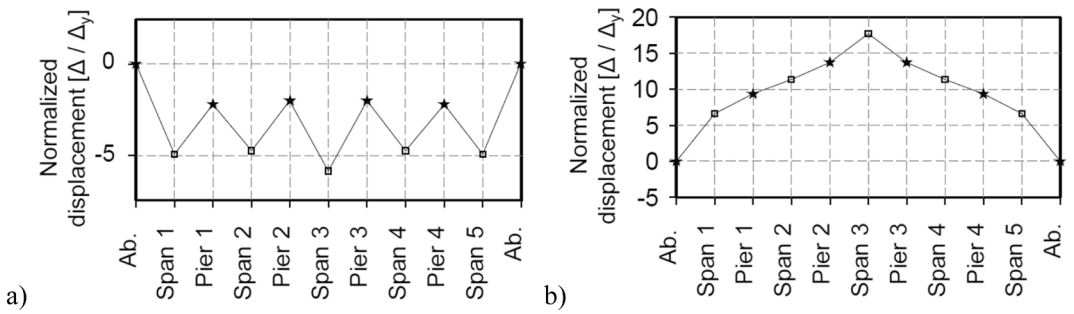

Fig. 7. Deformed shape for a 5-span bridge with: a) stiff pier; b) flexible pier.

median); however, the set of ground motions used is one of several sets that could possibly have been considered. Therefore, the results obtained with the set of ground motions were represented by a normal distribution where the demand was calculated as the mean (i.e. median of the normal distribution). From a design point of view, the mean provides slightly more conservativism compared with the median of the data set.

Note that a failure mode was not defined as part of this process. However, in practice, an upper ductility limit equal to twice the target ductility is usually recommended, given that BRBs are typically tested up to twice their design displacement. Therefore, given that the above results show significant scatter, to provide a reasonable margin of safety, it was deemed appropriate as a design goal to specify that 90% of the cases considered should develop ductilities lower than this upper limit. This 90% acceptance criteria is consistent with what is done in other recognized methodologies, such as FEMA P-695.

8.2. BRB demands

Fig. 6 shows the mean ductility demand for different BRBs in bridges with different numbers of spans and designed per the MM method with R equal to 4 for a BRB yield displacement equal to 0.138 in. Results shown are for BRBs connected to the abutment and piers for one-half of the bridge, and reporting results at each pier only for the BRB having the largest maximum ductility demand (given that both BRBs connecting to the same pier were constrained to have the same area, as described earlier, they did not necessarily have the same ductility demand). Note that uniform ductility demand at all locations was achieved in bridges with stiff piers since, in that case, the structures reduce to a series of identical SDOF systems. This is observed in Fig. 6 at the left end of the lines where all converge to a common point. When piers become flexible, the ductility demand increases in BRBs connected to the abutment while ductility demand in BRBs located at the piers generally reduces (with a few exceptions, particularly for the BRB located near the center of the bridge when the number of spans increases). This is because of the influence of higher modes in the bridge behavior. Although not presented here due to space constraints, similar behavior was observed in bridges designed with other values of the seismic reduction factor than presented here.

The behavior of the bridge, and therefore the variation in ductility demand, are related to the pier stiffness. To understand such variation, the deformation of bridges was studied. Fig. 7 shows the deformed structure for the cases of stiff piers and flexible piers, where the normalized values of longitudinal displacement are intentionally plotted in the transverse direction of the bridge to improve the visibility of the results given that the analysis is unidirectional. In the figure, stars represent the substructure, rectangles represent spans, and lines represent BRBs where a positive slope represents compression and a negative slope represents tension. Note that when piers are relatively rigid, spans displace more than piers and the BRBs connected to opposite sides of the same pier are in tension and in compression, respectively. In this case, it was also observed that all BRBs reached their maximum ductility at the same time. When piers are flexible, pier displacements tend to be of a magnitude that lies between that of its adjacent spans; as a result, BRBs connected to the same pier are both in compression or both in tension, and BRBs do not reach their maximum ductility simultaneously. The observed variation in the deformation history of each span indicates that performing capacity design considering BRB forces acting in the same direction is unduly conservative, because it ignores this non-simultaneous occurrence of peak forces in adjacent BRBs that results

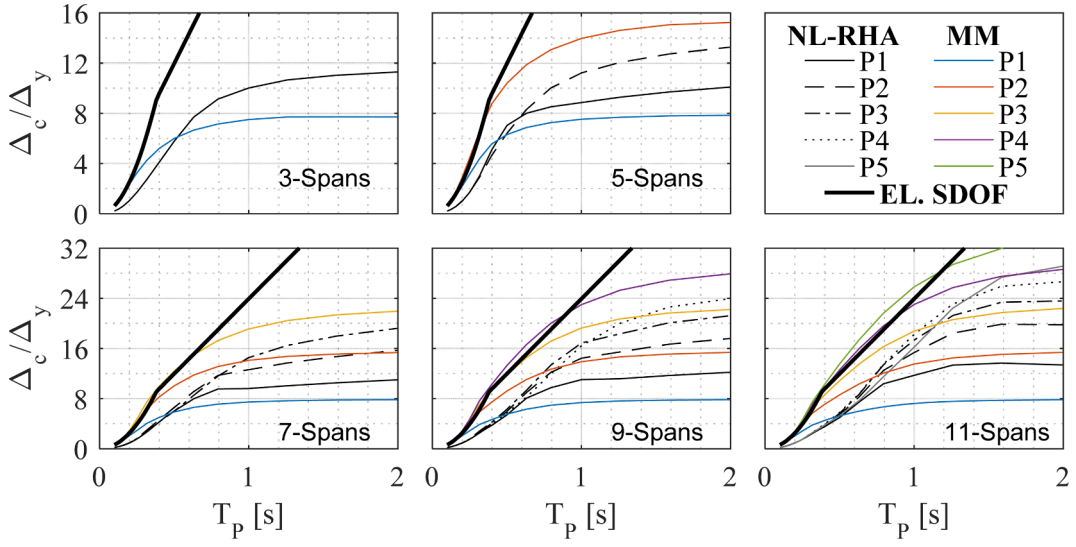

Fig. 8. Mean displacement in columns for bridges with BRBs designed with R = 4.

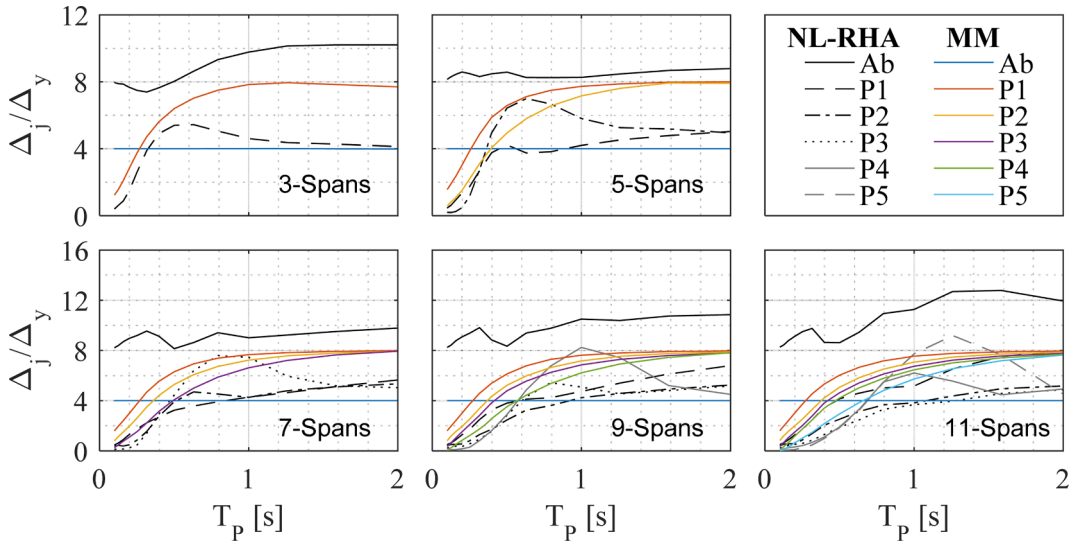

Fig. 9. Mean displacement in joints considering R = 1 in columns and R = 4 for BRBs.

due to the influence of higher modes. As an additional observation, note that displacement demands in piers are almost uniform when piers are rigid, whereas, in the case of flexible piers, the displacement demand increases for piers closer to the center of the bridge.

8.3. Column demands

One of the objectives of using bidirectional ductile end diaphragms is to reduce the demands in piers, which, in this study focusing on behavior in the longitudinal direction, can be established by comparing results obtained with the case where one end of the span is rigidly connected to the pier while the other is free (as done in conventional multi-span bridges). To compare the resulting column demands corresponding to both cases, columns were modeled to remain linear elastic in all analyses. Fig. 8 shows the demands in columns, Δ_c, for both cases and normalized in terms of the BRB yield displacement, Δ_y. For seamless continuity, results of NL-RHA are shown for bridges designed with R equal to 4. The bold line represents demand in piers for the case of conventional bridges where spans have a roller support at one end and a rigid connection to the pier cap at their other end; in this case, each pier behaves as a SDOF and the displacement demand is calculated directly from the displacement design spectrum. When comparing demands in both cases, it is observed that the use of BRB in the longitudinal direction effectively reduces displacement demands in columns compared with conventional bridges.

Fig. 8 also shows normalized displacement demand in columns calculated with MM for bridges designed with R = 4 and considering an overstrength equal to 4, which is equivalent to calculating elastic demands in columns (i.e., equivalent to those obtained if designing columns with R = 1). It is observed that displacements calculated with MM overestimate the demand in stiff piers and underestimate demand in piers close to the abutment for the case with flexibles piers. Note that, for such large overstrength, although the demands calculated for rigid piers are conservative (for this case the calculated ratios reach values up to 4 for extremely rigid piers), the demands obtained for flexible piers are up to 35% smaller than the demands obtained with NL-RHA for piers close to the abutment while demands in piers at the center of the bridge are larger than those obtained from NL-RHA. Consequently, a common overstrength factor cannot be used to define approximate demands in columns as a way to design them to remain elastic. This indicates that demands in columns cannot reliably be approximated using MM analysis and capacity design might be more appropriate for this purpose in a manner that remains to be determined.

8.4. Expansion joint demands and behavior

Another objective of the bidirectional ductile end diaphragm in the longitudinal direction is to limit the opening of the expansion joint to values manageable with regular low-cost expansion joint. Fig. 9 shows demands for joints, Δ_j, obtained from NL-RHA and normalized by the BRB yield displacement for bridges designed with R = 4. Note that the joint at the abutment is always the one with the largest demand, independently of the fact that the ductility demand is not always the largest in BRBs connected to the abutment. In all other joints the opening demand increases as the stiffness of the pier reduces (i.e. T_p increases), and the smallest demands at the interior joints are obtained when piers are rigid. However, conservatively, the demand in all joints can be considered equal to the elongation demand in BRBs. Note that calculating this demand in joints is important because earthquake demands can govern the joint design instead of temperature demands.

Demands in joints were also calculated with MM analysis considering an overstrength factor equal to 4 (i.e., equivalent to demands corresponding to R = 1). Results are shown with color lines in Fig. 9. Similarly to what was observed for columns, displacement demands at joints cannot be predicted accurately with MM for all BRBs. However, the demand in joints can be conservatively considered equal to the elongation corresponding to the maximum ductility demand obtained in BRBs along the bridge, which in most cases is equal or larger to the demand of the BRB connected to the abutment.

8.5. Sensibility for different models

As previously mentioned, the above results from non-linear analyses were obtained using the Menegotto Pinto (MP) model for the BRBs. The two additional models described earlier (namely, the Bouc Wen and the Modified Menegotto Pinto, MMP, models) were selectively used to analyze the sensitivity of the results to the choice of structural model. These two other nonlinear models introduce isotropic hardening which was intuitively expected to help better distribute ductility demands in BRBs along the length of the bridge. Results are shown in Fig. 10. Comparing the demands with respect to results obtained with the MP model, the figure shows that the Bouc Wen model results in demands similar to those obtained with the MP model, while the MMP model results in 30% larger demands. The trend in ductility demands with respect to the variation of the stiffness of the pier is similar for all models. Moreover, results for the MMP model show that demands for the BRBs located at the center of the bridge are larger than in other models,

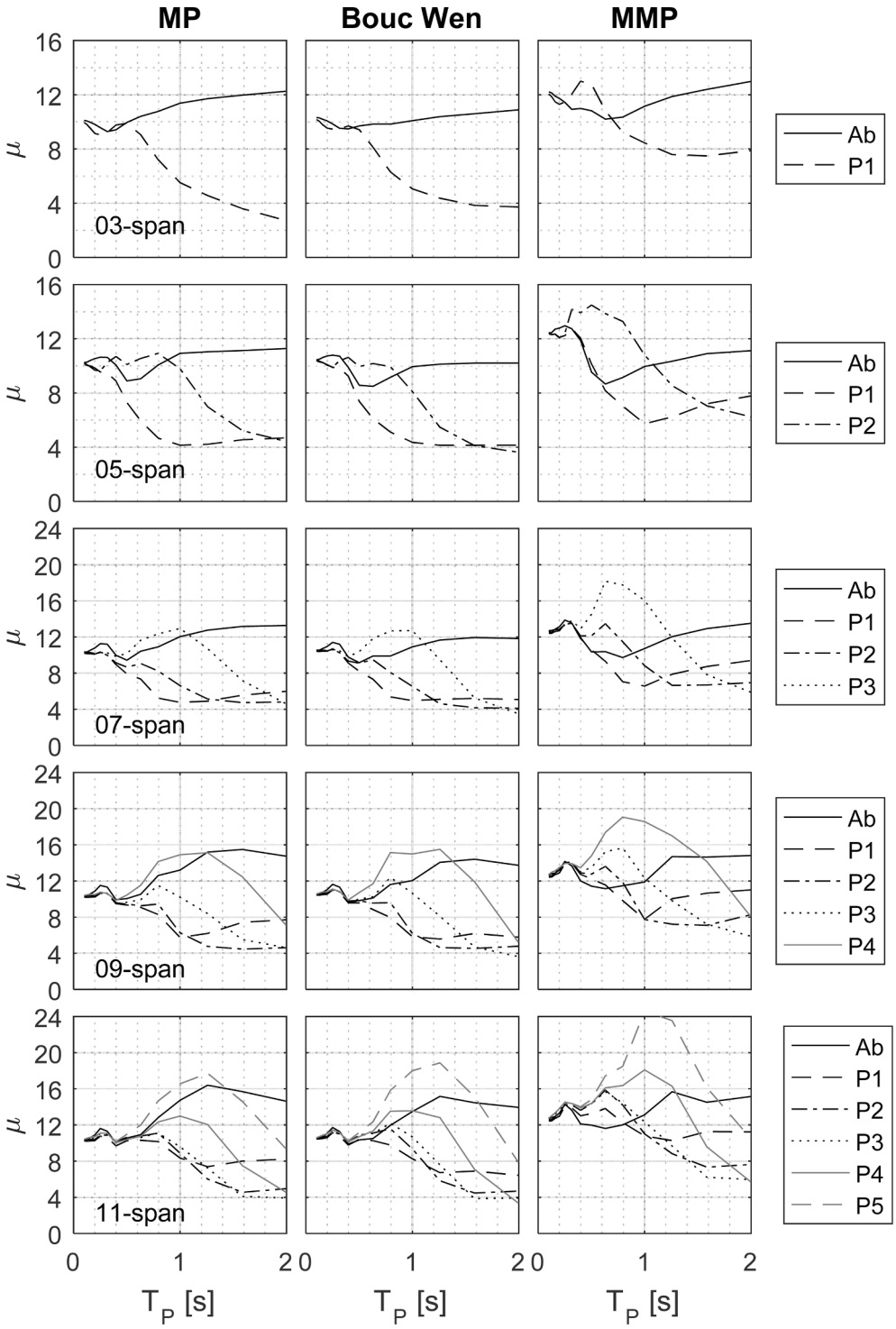

Fig. 10. Mean ductility demands in BRB for 3 to 11-span bridges designed with R = 5 and using the MP, Bouc Wen, and MPM material models.

especially in bridges with a large number of spans, counter to the original intuition. This increase in ductility demand was found to be attributable to the reduction in the post-yield stiffness that occurred, in spite of the strength increase due to isotropic hardening; to verify this, similar variations were observed when a single degree of freedom structure was analyzed.

Additionally, the maximum column displacements obtained with BRBs modeled with different material models were compared. The MP model without isotropic hardening generally produced larger column displacement demands compared to those obtained from the Bouc Wen model. For the MMP model, the mean displacement demands in columns were within ±10% of those obtained with the MP model, which is a negligible difference. As a result, it is found that displacement demands in columns are not highly sensitive to the nonlinear material model used here.

Although the MMP model more precisely represents the behavior of BRBs, some of the parameters of the model change based on the internal design of the device, which is more complicated than warranted for this study and for design purposes. Furthermore, since the goal of achieving uniform BRB ductility demands along the bridge was demonstrated by

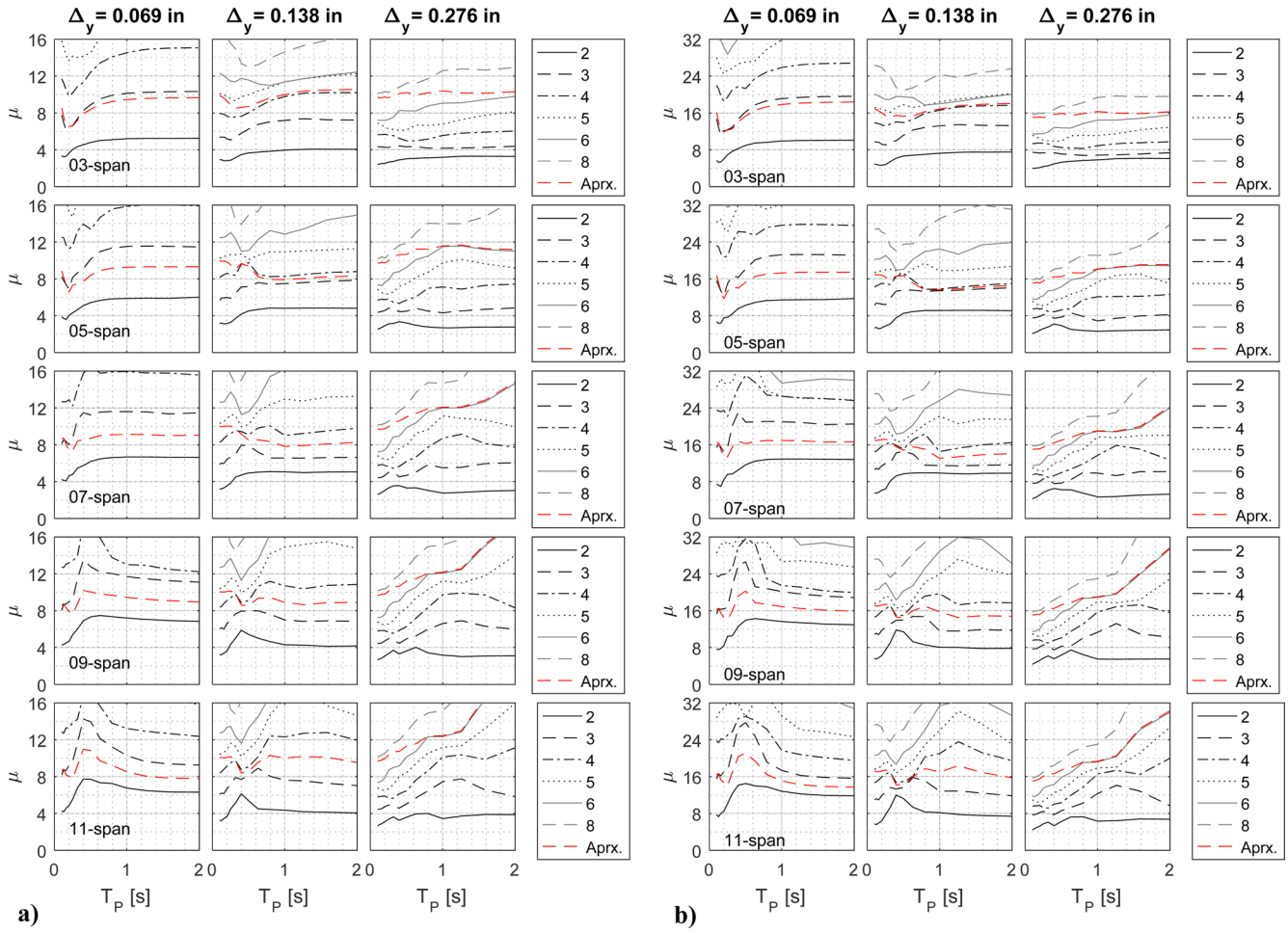

Fig. 11. Maximum demand ductilities in BRB for 3 to 11-span bridges designed with different R value factors and for different BRB yield displacement: a) mean demand; b) 90th percentile.

non-linear analysis to have not been achieved when the design is performed per the MM method, the design objective was revisited to focus instead on limiting the maximum BRB ductility demand along the length of the bridge. Therefore, for this case where BRBs with different internal designs would be obtained and BRB performance is limited to the maximum BRB ductility in the bridge, the MP model was deemed adequate and was used in all following analyses; in these subsequent analyses, the largest BRB mean demand ductility in any BRBs along the bridge length was reported as the ductility demand for each bridge.

8.6. Influence of different yield displacement

The influence of BRB yield displacement on achieving a given target ductility has a direct impact on the seismic force reduction factor used in the design. The reduction in yield displacement of a BRB typically goes along with a reduction of its stiffness, and therefore of the fundamental period of the bridge. It is well known that the assumption of equal elastic and inelastic seismic displacements is not valid for short period structures. This was demonstrated by many authors for SDOF systems (e.g. [44]). To account for this, in some design specifications, such as AASHTO LRFD [12], the seismic force reduction factor is adjusted accordingly. However, it was not known what would be this effect for multiple degrees of freedom bridges having BRBs. A limited parametric study was performed to investigate this further.

AASHTO LRFD proposes a displacement amplification to correct displacements of SDOF systems with short periods. The equation of the amplification factor, R_d, is defined as follow:

$$R_d = \begin{cases} \left(\frac{1}{R} - 1\right)\frac{1.25T_s}{T} + \frac{1}{R} & if \;\; T < 1.25T_s \\ 1 & otherwise \end{cases} \tag{7}$$

where, T is the period of the structure, and T_s is the largest period of the spectrum constant acceleration plateau. The ductility expected in a SDOF, μ_{SDOF}, is calculated as:

$$u_{SDOF} = R_d R \tag{8}$$

Multiplying Eq. (7) by R, substituting in Eq. (8), and solving for R:

$$R(T) = \begin{cases} (u_{SDOF} - 1)\frac{T}{1.25T_s} + 1 & if \;\; T < 1.25T_s \\ u_{SDOF} & otherwise \end{cases} \tag{9}$$

Eq. (9) can be used to calculate the reduction factor to design a SDOF system. Here, for the spectrum considered in this study, short-period structures are those with a period less than 1.25 T_s equal to 0.48 s.

From the parametric study, the maximum mean BRB ductilities obtained for bridges considering different yield displacements are shown in Fig. 11a. It is observed that to reach a specific target ductility, bridges with short yield displacements require a smaller reduction factor than bridges with large yield displacements (as is the case for SDOF systems). However, it is also observed that when the pier stiffness reduces, the period increases and the ductility demand also increases contrary to the behavior expected in a SDOF where for a given reduction factor the ductility reduces as the period increases. For instance, the 7-span bridge

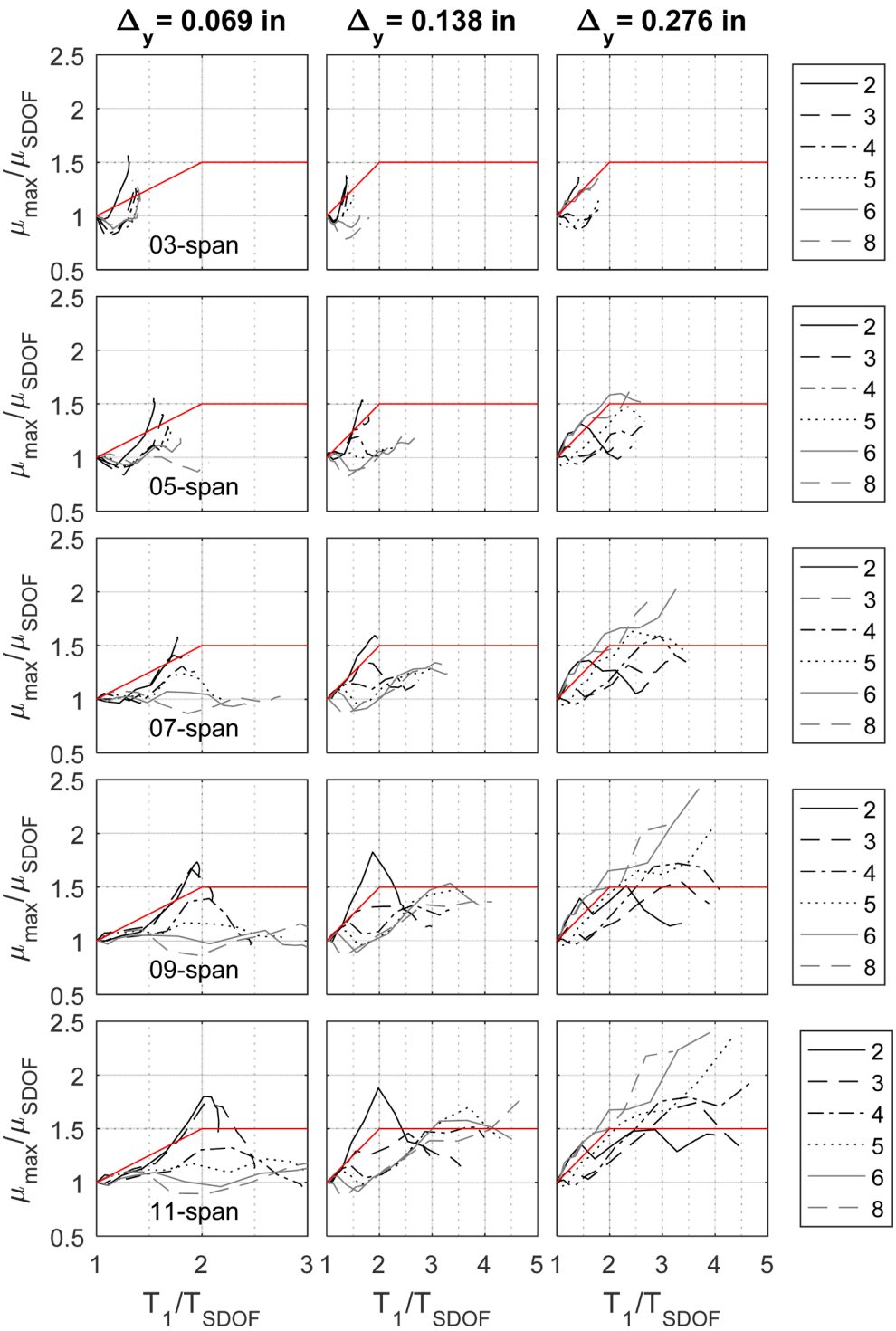

Fig. 12. Ratio between maximum ductility in the bridge to ductility of a SDOF vs the ratio between the period of the bridge to the period of a SDOF.

with yield displacement equal to 0.276 in, flexible pier with $T_p = 2$ s, and designed with R = 5 has a period equal to 1.50 s (although this period is not shown in the figure); a SDOF with this period is expected to reach a ductility equal to 5 (i.e. according to Eq. (7) and (8)), but the actual demand obtained from NL-RHA for the bridge with BRBs is twice this value, as shown in the figure. Also, note in Fig. 11b that the 90th percentile is generally less than twice the mean ductility, which meets the intent that BRBs be tested for twice their design displacement.

For the same R value, calculating the ratio of the maximum ductility for bridges having different pier stiffness over the ductility for the corresponding case with stiff piers (that is, itself, equivalent to a SDOF system), it was observed that this ratio is generally less than 1.5, as shown in Fig. 12. In fact, it was observed to increase from 1, to reach 1.5 when the period of the bridge considered here reached twice the period of the SDOF (represented by the period of the bridge with stiff piers). This observation is accurate for bridges with 7 spans and less. For a larger number of spans and larger yield displacements, the ratio increases above 1.5 for structures with periods greater than twice the period of the corresponding SDOF (i.e., bridges with flexible piers). Therefore, based on those results, it is proposed that the maximum BRB

ductility demand, μ_{max}, in the longitudinal BRBs of bridges designed by the MM method with a given R value, be approximated by the following equation:

$$\gamma_\mu = \frac{\mu_{max}}{\mu_{SDOF}} = 0.5 + 0.5\frac{T_1}{T_{SDOF}} \leq 1.5 \tag{10}$$

where T_1 is the fundamental period of the structure, and μ_{SDOF} and T_{SDOF} is the period and ductility of the SDOF system designed with the given R value, respectively. This approximation is used in the design procedure described in the next section.

9. Design procedure

Based on the above observations, a design procedure is proposed here to design BRBs in the longitudinal direction of regular multi-spans bridge having the configuration considered.

For the simplest and hypothetical case where piers are extremely rigid, each span with its BRBs behaves as a SDOF system. The SDOF system period for a given yield displacement is proposed here to be calculated using Eq. (9), derived from AASHTO LRFD [12]. However, the equation is valid for ductilities less than 5, as described by Riddell et al. [44]. Therefore, for larger ductilities, the equation can be modified as:

$$R(T) = \begin{cases} \left(\frac{u_{SDOF}}{\alpha_u} - 1\right)\frac{T}{1.25T_s} + 1 & if \;\; T < 1.25T_s \\ \frac{u_{SDOF}}{\alpha_u} & otherwise \end{cases} \tag{11}$$

where α_u is a factor that is used with ductilities larger than 5, and is otherwise taken as equal to 1. For ductilities up to 10, it was obtained from NL-RHA of SDOF systems with the set of ground motion used here that α_u can be defined as:

$$1.0 \leq \alpha_u = 0.06\mu_{SDOF} + 0.7 \leq 1.3 \tag{12}$$

The amplification of displacement demand due to a short period, R_d, is calculated with

$$R_d(T) = \frac{\mu_{SDOF}}{R(T)} \tag{13}$$

The inelastic spectral displacement is calculated with

$$S_d(T) = R_d(T)\cdot g\cdot Sa(T)\cdot\left(\frac{T}{2\pi}\right)^2 = \frac{\mu_{SDOF}}{R(T)}\cdot g\cdot Sa(T)\cdot\left(\frac{T}{2\pi}\right)^2 \tag{14}$$

where $Sa(T)$ is the design spectrum, and g is the gravity acceleration. The period of the SDOF, T_{SDOF}, can be obtained by solving the following equation:

$$\Delta_y\cdot\mu_{SDOF} = S_d(T_{SDOF}) = \frac{\mu_{SDOF}}{R(T)}\cdot g\cdot Sa(T)\cdot\left(\frac{T}{2\pi}\right)^2 \tag{15.1}$$

$$\Delta_y = \frac{g\cdot Sa(T_{SDOF})}{R(T_{SDOF})}\cdot\left(\frac{T_{SDOF}}{2\pi}\right)^2 \tag{15.2}$$

The solution could be easily solved graphically by drawing the inelastic spectral displacement and locating the period for the target displacement.

For the case of flexible piers, the proposed design procedure is iterative and the solution steps are as follows:

1. Define the maximum ductility, μ_{max}, assume a period of the structure, T_1, and the period of the SDOF, T_{SDOF}.
2. Calculate γ_u with Eq. (10) and the ductility in the SDOF with:

$$\mu_{SDOF} = \frac{u_{max}}{\gamma_u} \tag{16}$$

3. Calculate α_u per Eq. (12).
4. Solve Eq. (15.2) for T_{SDOF} and calculate the reduction factor $R(T_{SDOF})$ with Eq. (11).
5. Design the structure using the MM method and calculate the period of the structure.
6. Convergence is reached when the absolute difference between the period from step 5 and the period used in step 2 is smaller than an acceptable tolerance. Therefore; if the absolute difference between periods is larger than the defined tolerance, return to step 2 and iterate with the new period; otherwise, a satisfactory solution has been reached.

As an example, results obtained using the above proposed procedure for a target ductility equal to 10 are shown in Fig. 11 by a dashed red line. The values shown were calculated using linear interpolation between results from NL-RHA. The period used in step 1 for the target ductility was interpolated between periods of bridges used in NL-RHA, then calculations followed the procedure described above. An R value was calculated, the structure was designed with MM, and the new period for that R was obtained. To obtain the final designed structure, the process required a few iterations until convergence of period was obtained, and for the last R value, again the maximum ductility demand in the structure was interpolated between NL-RHA results. Note that ductility demands are in some cases larger than the target ductility. However, in the 90th percentile case, BRBs ductilities are less than twice the target ductility for bridges up to 7 spans (except for the 7-span bridge where T_p is larger than 1.5, for which the 90th percentile ductility demand ranges from 20 to 24, slightly exceeding the design objective). Therefore, those designs are deemed acceptable since BRBs are tested for up to 2 times the design displacement and only 10% of the cases considered here resulted in values of ductility demands exceeding this criterion.

10. Conclusions

Simply supported regular multi-span bridges having BRBs in the longitudinal direction were studied considering two different BRB configurations (as one part of a bidirectional ductile end diaphragm concept). The configuration with BRBs connecting spans to their adjacent piers and abutments was found to be advantageous because it generally required smaller BRB cross-section areas than the configuration in which BRBs connected spans to each other but not to the piers. Results from NL-RHA showed that this configuration also resulted in smaller force demands in columns compared to conventional designs (i.e., without BRBs) where spans are rigidly connected to piers at one of their ends, when the objective is to keep columns elastic. Moreover, in bridges with BRBs, displacement demands in expansion joints were also smaller and limited to a magnitude that can be accommodated with regular small to medium range expansion joints; this can also be helpful to prevent span unseating failure. The demands in columns and expansion joints are driven by the elongation of the BRBs, which underscores the need for a design procedure that can control the maximum ductility demands of the BRBs.

A parametric study was conducted to determine if the multimode design method was a viable procedure to design bridges with BRBs in the longitudinal direction. It was found that achieving uniform ductility demand in the BRBs located along the length of the bridge was not possible with this method, but that it could be used to limit the maximum ductility demand in these BRBs. Based on these observations,

a procedure using the multimode method was proposed to design BRBs such that one BRB in the bridge reaches the target ductility demand while ductility demands are smaller in the other BRBs. At this time, this procedure is limited in applicability to the straight bridges considered in this study, namely having simply supported spans of equal mass supported on piers of equal stiffness, as sometimes found in highway bridges. It was found that the proposed design procedure provides acceptable accuracy for target ductilities up to 10 and bridges with less than 7 spans, independently of the BRB yield displacement; for bridges with a larger number of spans, the accuracy of the results is reduced. It was also found that predicted ductility demands could be 30% larger when using a Modified Menegotto Pinto hysteretic material model rather than the Bouc Wen and Menegotto Pinto models often used for BRBs in non-linear analysis, but variations in displacement demands in columns were found to be negligible when different BRB material models were used.

Overall, the results obtained in this study demonstrate that, in bridges using the bidirectional ductile end diaphragm concept, seismic demands in the longitudinal direction can be effectively addressed by connecting spans to their adjacent piers/abutments with BRBs. This is achieved by limiting yielding to the BRBs and protecting the rest of the super and substructures. However, designs performed using the elastic multimode analysis procedure were found to require several iterations until convergence is reached. The resulting elastic demands in columns were not always conservative, and when they were conservative, they generally differed significantly from those obtained with NL-RHA. This provides opportunities for future research to simplify the design of these bridges while still achieving satisfactory seismic performance. Future research will also be required to investigate the adequacy of the proposed concept for bridges having variable span lengths and pier stiffnesses, as well as continuous bridges and other irregular configurations.

CRediT authorship contribution statement

Homero Carrion-Cabrera: Conceptualization, Methodology, Software, Validation, Formal analysis, Investigation, Data curation, Writing – original draft, Writing – review & editing, Visualization. **Michel Bruneau:** Conceptualization, Validation, Investigation, Resources, Writing – review & editing, Supervision, Project administration, Funding acquisition.

Declaration of Competing Interest

The authors declare that they have no known competing financial interests or personal relationships that could have appeared to influence the work reported in this paper.

Acknowledgements

The Fulbright program, SENESCYT Ecuador, and the University at Buffalo are acknowledged for their financial support through a scholarship for the first author. This study was also sponsored by the Transportation Research Board of the National Academies under the TRB-IDEA Program (NCHRP-215). However, any opinions, findings, conclusions, and recommendations presented are those of the authors alone. The Academy and U.S. Government do not necessarily concur with, endorse, or adopt the findings, conclusions and recommendations either inferred or expressly stated here.

Appendix A

The value of the parameters used in this study for the different steel models used in OpenSees are listed in Table 2. The parameter names/variables listed in this table are the same as those used in the definition of each model on their respective OpenSees webpages.

Table 2
Material Parameters.

Menegotto Pinto model		SteelMPF		Bouc Wen model	
Parameter	Value	Parameter	Value	Parameter	Value
fy	50 ksi	fyp	50 ksi	alpha	0.0065
E0	29,000 ksi	fyn	50 ksi	ko	29,000
b	0.03	E0	29,000 ksi	n	1.0
R0	18	bp	0.006	gamma	0.0
cR1	0.925	bn	0.021	beta	505
cR2	0.95	R0	30	Ao	1
		CR2	0.915	deltaA	-0.00599
		CR2	0.150	deltaNu	0.00
		a1	0.041	deltaEta	0.0141
		a2	1.0		
		a3	0.037		
		a4	1.0		

References

[1] Aiken I, Clark P, Tajirian F, Kasai K, Kimura I, Ko E. Unbonded braces in the United States—Design studies, large-scale testing, and the first building application. In: Proceedings of the International Post-SMiRT Conference Seminar, Korea Earthquake Engineering Research Center, vol. I; 1999. p. 317–37.
[2] AISC 341. Seismic Provisions for Structural Steel Buildings. Chicago, Illinois, USA: American Institute of Steel Construction (AISC); 2016.
[3] Lanning J, Benzoni G, Uang C-M. Using buckling-restrained braces on long-span bridges. II: Feasibility and development of a near-fault loading protocol. J Bridge Eng 2016;21(5):04016002. https://doi.org/10.1061/(ASCE)BE.1943-5592.0000804.
[4] Kanaji H, Hamada N, Ishibashi T, Amako M, Oryu T. Design and performance tests of buckling restrained braces for seismic retrofit of a long-span bridge. 21th US–Japan bridge engineering workshop. Panel on wind and seismic effects. 2005.
[5] Zahrai SM, Bruneau M. Ductile end-diaphragms for seismic retrofit of slab-on-girder steel bridges. J Struct Eng 1999;125(1):71–80.
[6] Alfawakhiri F, Bruneau M. Local versus global ductility demands in simple bridges. J Struct Eng 2001;127(5):554–60.
[7] AASHTO, AASHTO Guide Specifications for LRFD Seismic Bridge Design. 2nd ed. Revision 2015. AASHTO; 2011.
[8] Carden LP, Itani AM, Buckle IG. Seismic performance of steel girder bridges with ductile cross frames using buckling-restrained braces. J Struct Eng 2006;132(3):338–45.
[9] Celik OC, Bruneau M. Seismic behavior of bidirectional-resistant ductile end diaphragms with buckling restrained braces in straight steel bridges. Eng Struct 2009;31(2):380–93.
[10] Wei X, Bruneau M. Experimental investigation of buckling restrained braces for bridge bidirectional ductile end diaphragms. J Struct Eng 2018;144(6):04018048. https://doi.org/10.1061/(ASCE)ST.1943-541X.0002042.
[11] Pantelides CP, Ibarra L, Wang Y, Upadhyay A, Consortium MP. Seismic rehabilitation of skewed and curved bridges using a new generation of buckling restrained braces; 2016.
[12] AASHTO. AASHTO LRFD Bridge Design Specifications. 8th Edition ed.; 2017.
[13] Bruneau M, Uang C-M, Sabelli SR. Ductile design of steel structures. McGraw Hill; 2011.
[14] Clark P, Aiken I, Kasai K, Ko E, Kimura I. Design procedures for buildings incorporating hysteretic damping devices; 1999.
[15] Watanabe A, Hitomi Y, Saeki E, Wada A, Fujimoto M. Properties of brace encased in buckling-restraining concrete and steel tube. Proceedings of ninth world conference on earthquake engineering. 1988.
[16] Tsai K-C, Hwang Y-C, Weng C-S, Shirai T, Nakamura H. Experimental tests of large scale buckling restrained braces and frames. Proceedings, Passive Control Symposium. 2002.
[17] Fahnestock LA, Ricles JM, Sause R. Experimental evaluation of a large-scale buckling-restrained braced frame. J Struct Eng 2007;133(9):1205–14.
[18] Takeuchi T, Ozaki H, Matsui R, Sutcu F. Out-of-plane stability of buckling-restrained braces including moment transfer capacity. Earthquake Eng Struct Dyn 2014;43(6):851–69.
[19] Zaboli B, Clifton G, Cowie K. BRBF and CBF gusset plates: Out-of-plane stability design using a simplified Notional Load Yield Line (NLYL) method. SESOC J 2018;31(1):64.
[20] MacRae G, Lee C-L, Vazquez-Coluga S, Cui J, Alizadeh S, Jia L-J. BRB system stability considering frame out-of-plane loading and deformation zone. Bull NZ Soc Earthq Eng 2021;XX.
[21] Iwata M, Kato T, Wada A. Buckling-restrained braces as hysteretic dampers. Behavior of steel structures in seismic areas; 2000. p. 33-8.
[22] Murphy C, Pantelides CP, Blomgren H-E, Rammer D. Development of Timber Buckling Restrained Brace for Mass Timber-Braced Frames. J Struct Eng 2021;147(5):04021050. https://doi.org/10.1061/(ASCE)ST.1943-541X.0002996.
[23] Chou C-C, Chen S-Y. Subassemblage tests and finite element analyses of sandwiched buckling-restrained braces. Eng Struct 2010;32(8):2108–21.

[24] Saxey B, Vidmar Z, Reynolds M, Uang C-M. A predictive low-cycle fatigue model for buckling restrained braces. In: 17th World Conference on Earthquake Engineering: Sendai, Japan; 2020.
[25] Sabelli R, Mahin S, Chang C. Seismic demands on steel braced frame buildings with buckling-restrained braces. Eng Struct 2003;25(5):655–66.
[26] Tremblay R, Poncet L, Bolduc P, Neville R, DeVall R. Testing and design of buckling restrained braces for Canadian application. Proceedings of the 13th world conference on Earthquake Engineering. 2004.
[27] Teran-Gilmore A, Virto-Cambray N. Preliminary design of low-rise buildings stiffened with buckling-restrained braces by a displacement-based approach. Earthquake Spectra 2009;25(1):185–211.
[28] Guerrero H, Ji T, Teran-Gilmore A, Escobar JA. A method for preliminary seismic design and assessment of low-rise structures protected with Buckling-Restrained Braces. Eng Struct 2016;123:141–54.
[29] Kiggins S, Uang C-M. Reducing residual drift of buckling-restrained braced frames as a dual system. Eng Struct 2006;28(11):1525–32.
[30] Tsai K-C, Hsiao P-C, Wang K-J, Weng Y-T, Lin M-L, Lin K-C, et al. Pseudo-dynamic tests of a full-scale CFT/BRB frame—Part I: Specimen design, experiment and analysis. Earthquake Eng Struct Dyn 2008;37(7):1081–98.
[31] Tsai KC, Hsiao PC. Pseudo-dynamic test of a full-scale CFT/BRB frame—Part II: Seismic performance of buckling-restrained braces and connections. Earthquake Eng Struct Dyn 2008;37(7):1099–115.
[32] Lanning J, Benzoni G, Uang C-M. Using buckling-restrained braces on long-span bridges. I: full-scale testing and design implications. J Bridge Eng 2016;21(5): 04016001.
[33] Wei X, Bruneau M. Buckling restrained braces applications for superstructure and substructure protection in bridges. State University of New York at Buffalo; 2016.
[34] Haukaas T, Der Kiureghian A. Finite element reliability and sensitivity methods for performance-based earthquake engineering. Peer; 2003(April). p. 266-6.
[35] Black CJ, Makris N, Aiken ID. Component Testing, Seismic Evaluation and Characterization of Buckling-Restrained Braces. J Struct Eng 2004;130(6):880–94.
[36] Filippou FC, Bertero VV, Popov EP. Effects of bond deterioration on hysteretic behavior of reinforced concrete joints. EERC; 1983.
[37] McKenna F, Fenves GL, Scott MH. Open system for earthquake engineering simulation. Berkeley, CA: University of California; 2000.
[38] Charney FA. Unintended consequences of modeling damping in structures. J Struct Eng 2008;134(4):581–92.
[39] The Mathworks Inc. MATLAB R2016b; 2016.
[40] FEMA, Quantification of Building Seismic Performance Factors., C. Applied Technology Council for the Federal Emergency Management Agency: Redwood City, USA., Editor; 2009.
[41] Mahin SA, Lin J. Construction of inelastic response spectra for single-degree-of-freedom systems. Earthquake Engineering Center. Berkeley: University of California; 1983.
[42] Caughey T. Classical normal modes in damped linear dynamic systems. J Appl Mech 1960;27(2):269–71.
[43] Fischinger M, Isakovic T, Fajfar P. Seismic Analysis of Viaduct Structures-Which Method to Choose?. Proceedings of the International Workshop on Seismic Design Methodologies for the Next Generation of Code. 1997.
[44] Riddell R, Hidalgo P, Cruz E. Response modification factors for earthquake resistant design of short period buildings. Earthquake spectra 1989;5(3):571–90.